Journal of Sound and Vibration (1999) **222**(4), 565–578
Article No. jsvi.1998.2039, available online at http://www.idealibrary.com on IDEAL

RESPONSES OF NEAR-OPTIMAL, CONTINUOUS HORIZONTALLY CURVED BEAMS TO TRANSIT LOADS

J. F. WILSON

Department of Civil and Environmental Engineering, Duke University, Durham, NC 27708-0287, *U.S.A.*

Y. WANG

Department of Civil Engineering, Northern Jiaotong University, Beijing 100044, *People's Republic of China*

AND

I. THRELFALL

Duke University, Durham, NC 27708-0287, *U.S.A.*

(*Received* 16 *January* 1998, *and in final form* 9 *November* 1998)

1. INTRODUCTION

In the historical study of Tan and Shore [1], dynamic responses were predicted for a single, simply supported, horizontally curved beam subjected to a constant vertical point force moving at constant speed. In that study, the two governing fourth order differential equations, originally derived by Vlasov [2] in static form, were modified to include the span inertia and the transit force. Later, Huang *et al.* [3, 4], whose citations include related studies on curved spans, used discrete numerical analyses to calculate the dynamic responses of simple, horizontally curved bridges to sprung masses simulating transit vehicles. For the investigations herein, series solutions to Vlasov's equations of motion are presented, where those equations are modified to include a constant transit torque moving at constant speed, simulating the centrifugal loading of a transit vehicle supported by the curved span. The investigations herein also employ the results of the companion paper by Snyder and Wilson [5], which presented the coupled bending and twisting out-of-plane free vibration frequencies and mode shapes for continuous curved spans over multiple pier supports. Illustrated in the present study are the critical 3-span curved beam deflection and rotation responses for a 90-degree bend, cast as a function of non-dimensional transit speed and pier spacing. Near-optimal pier spacings are recommended for response reduction. In addition, an experimental system is described and experimental results are shown to complement the theory. These results may be useful in the efficient and dynamically sound design of future transit structures, serving to complement results of bridge designers who may employ dynamic

0022–460X/99/190565 + 14 $30.00/0

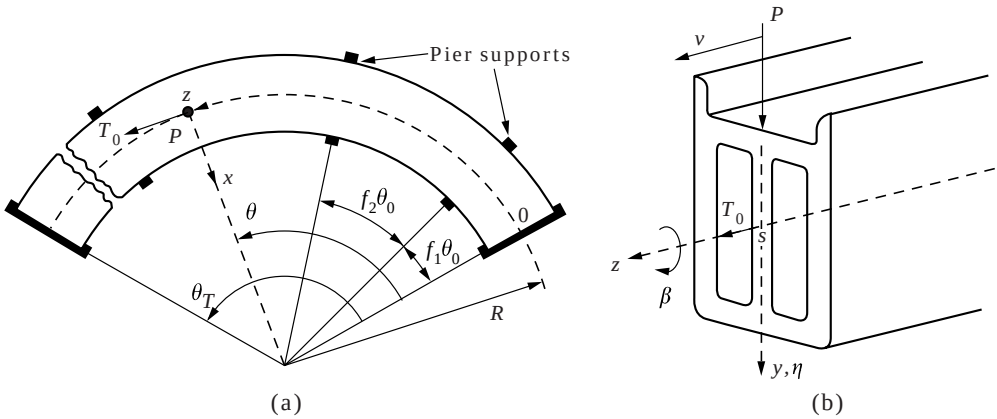

Figure 1. (a) Plan view and (b) a typical cross-section of the continuous horizontally curved span showing the co-ordinate system. The transit loadings P and T_0 are both located at $z = R\theta$.

finite element analysis to compute span stresses, including the effects of sprung transit vehicles.

2. THE MATHEMATICAL MODE

Shown in Figures 1(a) and (b) are the geometry, the co-ordinate system, and the loadings for the curved beam, which is a uniform, continuous span of constant horizontal radius R in the xz-plane. The shear center s and the centroid of the cross-section are assumed to be coincident. This continuous span has a total included angle θ_T between the extreme end supports and has N clear segments between the $N+1$ supports. For reference purposes, L is defined as the mean centerline length of the clear spans, where $L = R\theta_T/N = R\theta_0$. The pier spacing for the ith clear segment is defined as $f_i R\theta_0$ where the multipliers f_i for $i = 1, 2, \ldots, N$ are determined later in the paper.

As shown in Figure 1, the span is loaded with a constant vertical point load P with its line of action through s. This load traverses the span at constant speed v and is located at z along the span centerline, where z is the curvilinear co-ordinate measured to the left from the right end of the span along the span's centerline. Also located at s and acting along z is the companion transit torque T_0, which models the twisting of the cross-section due to a vehicle's centrifugal loading acting in the negative x direction: either directly against the outer wall of the span, or on the span surface from tire friction in the absence of this restraining wall.

The governing equations for the vertical motion $\eta = \eta(z, t)$ and the rotation of the cross-section $\beta = \beta(z, t)$ were originally derived by Vlasov [2], who assumed elastic action with small strains and who employed the left-handed co-ordinate system (x, y, z) of Figure 1. The nomenclature for the governing, coupled equations that follow is generally that used in the companion paper by Snyder and Wilson [5]:

$$\left(EI+\frac{D}{R^2}\right)\frac{\partial^4\eta}{\partial z^4}-\frac{C}{R^2}\frac{\partial^2\eta}{\partial z^2}+\frac{D}{R}\frac{\partial^4\beta}{\partial z^4}-\frac{EI+C}{R}\frac{\partial^2\beta}{\partial z^2}+m\frac{\partial^2\eta}{\partial t^2}=P_0\delta(z-vt), \qquad (1)$$

$$\frac{D}{R}\frac{\partial^4\eta}{\partial z^4}-\frac{EI+C}{R}\frac{\partial^2\eta}{\partial z^2}+D\frac{\partial^4\beta}{\partial z^4}-C\frac{\partial^2\beta}{\partial z^4}+\frac{EI}{R^2}\beta+mr^2\frac{\partial^2\beta}{\partial t^2}=-T_0\delta(z-vt), \qquad (2)$$

in which t is time. The point loadings, characterized by the Kronecker delta, are P_0 and T_0 at $z=vt$, and are zero otherwise. The bending stiffness about the x-axis is EI, the torsion stiffness for rotation about the z-axis is $C=GJ$, and the warping constant for the cross-section is $D=EI_w$. Here, E and G are Young's modulus and the shear modulus, respectively; I is the second area moment about the x-axis; J is St Venant's torsion constant [6]; and I_w is the warping factor. As discussed in reference [6], I_w has a computed, non-zero value for thin-walled open sections such as I-beams and channels; but is zero for closed sections such as box beams, most flat plates, and all circular sections. In the inertial terms, m is the span mass per unit length and $r=(I_p/A)^{1/2}$ is radius of gyration of the cross-section in which I_p is the second area moment with respect to the z-axis and A is the cross-sectional area.

The governing equations are cast in non-dimensional form using three parameters based on a reference span, which is a single, simply supported straight beam with bending stiffness EI, length L, and mass per unit length m. Those three parameters are the fundamental bending frequency p_0 (rad/s), the peak midspan deflection η_s under P_0, and the passage frequency ω (rad/s) for the traversing load P_0, which are defined respectively by

$$p_0=\left(\frac{\pi^4EI}{mL^4}\right)^{1/2}, \qquad \eta_s=\frac{P_0L^3}{48EI}, \qquad \omega=\frac{\pi v}{L}. \qquad (3)$$

Further, the non-dimensional system parameters for the curved configuration are defined as follows. The stiffness and geometric parameters are

$$\bar{C}=C/(EI), \quad \bar{D}=D(EIR^2), \quad f_1,f_2,\ldots,f_N, \quad \zeta=r/R, \quad \theta_0=L/R=\theta_T/N. \qquad (4)$$

The time and frequency parameters are

$$\bar{t}=\omega t, \qquad \bar{p}=p/p_0, \qquad \Omega=\omega/p_0=\pi v/(Lp_0), \qquad (5)$$

where p represents the free vibration frequencies for the curved configuration. The co-ordinate parameters are

$$\bar{z}=z(\bar{t})=z/L, \qquad \bar{\beta}=\beta(\bar{z},\bar{t})=\beta R/\eta_s, \qquad \bar{\eta}=\eta(\bar{z},\bar{t})=\eta/\eta_s. \qquad (6)$$

The load parameters are

$$\bar{P}=48\delta_0(\bar{z}-\bar{t}/\pi), \qquad \bar{T}=T_0\bar{P}/(RP_0), \qquad (7)$$

where $\delta_0=1$ at $\bar{z}=\bar{t}/\pi$ and $\delta_0=0$ otherwise.

With equations (3)–(7), the governing equations (1) and (2) become

$$(1+\bar{D})\frac{\partial^4\bar{\eta}}{\partial\bar{z}^4}-\theta_0^2\bar{C}\frac{\partial^2\bar{\eta}}{\partial\bar{z}^2}+\bar{D}\frac{\partial^4\bar{\beta}}{\partial\bar{z}^4}-\theta_0^2(1+\bar{C})\frac{\partial^2\bar{\beta}}{\partial z^2}+\pi^4\Omega^2\frac{\partial^2\bar{\eta}}{\partial\bar{t}^2}=\bar{P}, \tag{8}$$

$$\bar{D}\frac{\partial^4\bar{\eta}}{\partial\bar{z}^4}-\theta_0^2(1+\bar{C})\frac{\partial^2\bar{\eta}}{\partial\bar{z}^2}+\bar{D}\frac{\partial^4\bar{\beta}}{\partial\bar{z}^4}+\pi^4\Omega^2\zeta^2\frac{\partial^2\bar{\beta}}{\partial\bar{t}^2}-\bar{C}\theta_0^2\frac{\partial^2\bar{\beta}}{\partial\bar{z}^2}+\theta_0^4\bar{\beta}=-\bar{P}\bar{T}. \tag{9}$$

3. SOLUTIONS FOR TRANSIT LOADING

For continuous horizontally curved beams, the general methods for computing the free vibration frequencies $p=p_n$, with $n=1, 2, \ldots$, and their corresponding mode shapes $\bar{W}_n=\bar{W}_n(\bar{z})$, based on the homogeneous forms of equations (8) and (9), were derived in general by Snyder and Wilson [5]. In that work, which employs the present nomenclature, the boundary conditions, the continuity conditions, and the methodology leading to solutions for p and $\bar{W}_n$ are presented in great detail and thus will not be repeated herein. Using the frequencies and mode shapes so calculated, solutions to the non-homogeneous forms of equations (8) and (9), or for non-zero transit point loads, may be found by the normal mode method with solutions in the forms

$$\bar{\eta}=\sum_{n=1}^{\infty}Z_n\bar{W}_n, \qquad \bar{\beta}=\sum_{n=1}^{\infty}\Theta n\bar{W}_n, \tag{10}$$

in which $Z_n=Z_n(\bar{t})$ and $\Theta_n=\Theta_n(\bar{t})$. The operator notations $\cdot=\mathrm{d}/\mathrm{d}\bar{t}$ and $'=\mathrm{d}/\mathrm{d}\bar{z}$ are used with equations (10) to rewrite equations (8) and (9). Each of those equations is then multiplied by $\bar{W}_m=\bar{W}_m(\bar{z})$ and each term is then integrated over the range $0\leqslant\bar{z}\leqslant R\theta_T/L$. Use is then made of the orthogonal properties of $\bar{W}_n$, or

$$\sum\int\bar{W}_m\bar{W}_n\,\mathrm{d}\bar{z}=\begin{cases}0, & \text{for } m\neq n,\\ B_0, & \text{for } m=n,\end{cases} \tag{11}$$

$$\sum\int\bar{W}_m\bar{W}_n''\,\mathrm{d}\bar{z}=\begin{cases}0, & \text{for } m\neq n,\\ B_2, & \text{for } m=n,\end{cases} \tag{12}$$

$$\sum\int\bar{W}_m\bar{W}_n''''\,\mathrm{d}\bar{z}=\begin{cases}0, & \text{for } m\neq n,\\ B_4, & \text{for } m=n,\end{cases} \tag{13}$$

In the above three equations, integration is piecewise over each span segment, and the summation is for all span segments.

The results lead to the following two coupled second order differential equations in the single independent variable $\bar{t}$:

$$\begin{bmatrix} m_1 & 0 \\ 0 & m_2 \end{bmatrix} \begin{bmatrix} \ddot{Z}_n \\ \ddot{\Theta}_n \end{bmatrix} + \begin{bmatrix} a_{11} & a_{12} \\ a_{21} & a_{22} \end{bmatrix} \begin{bmatrix} Z_n \\ \Theta_n \end{bmatrix} = 48 \begin{bmatrix} \bar{W}_n(\bar{t}/\pi) \\ -\bar{T}\bar{W}_n(\bar{t}/\pi) \end{bmatrix}, \tag{14}$$

in which the constants are given by

$$\begin{gathered} m_1 = \pi^4 \Omega^2 B_0, \qquad m_2 = m_1 \zeta^2, \\ a_{11} = (1 + \bar{D})B_4 - \theta_0^2 \bar{C} B_2, \qquad a_{21} = a_{12} = \bar{D} B_4 - \theta_0^2 (1 + \bar{C}) B_2, \\ a_{22} = \bar{D} B_4 - \theta_0^2 \bar{C} B_2 + \theta_0^4 B_0. \end{gathered} \tag{15}$$

The following initial conditions at $\bar{t} = 0$ are applied to the solutions of equations (14), conditions that assure that the continuous span is flat and at rest just before the transit loads are applied:

$$Z_n(0) = \dot{Z}_n(0) = \Theta_n(0) = \dot{\Theta}_n(0) = 0. \tag{16}$$

Given the coefficients of equations (15), the mode shapes $\bar{W}_n$, and the transit torque $\bar{T}$, equations (14) may be solved numerically for a sufficient number of mode shapes, typically for $n = 1, 2, \ldots, 6$, and with these solutions the time-varying vertical deflection $\bar{\eta}$ and rotation $\bar{\beta}$ may be calculated from equations (10) at a material point $\bar{z}$ on the span.

4. NEAR-OPTIMAL SPANS

A near-optimal continuous span with N segments, where each segment i has length $f_i R\theta_0$, is now defined by a set of span multipliers f_i, subjected to the following four constraints.

(1) The extreme ends of the span rest on simple supports.
(2) The overall span length $R\theta_T = LN$ is fixed, or $f_1 + f_2 + \cdots f_N = N$.
(3) The span segment lengths are symmetric about the midlength, or $f_i = f_{N+1-i}$. This assumption of symmetry eliminates any directional bias, so that the moving load (the vehicle) may enter the span from either end, which is a practical consideration.
(4) As the vertical load traverses the whole configuration at crawl speed, a peak vertical deflection δ_i occurs under the load at each mid-segment i. For the near-optimal configuration, all of the δ_i values are identical, and each f_i is chosen to make this so.

While a span designed with such constraints is the static optimal, it is realized that this span may not necessarily meet the fourth criterion for v over a range of elevated speeds, and thus the *near-optimal* designation was chosen. The assumption is that that transit loads at elevated speeds on near-optimal spans will generally result in smaller maximum dynamic responses than for spans of equal length segments (all $f_i = 1$), other system parameters remaining the same. Such was the case for the counterpart problem of straight, continuous spans investigated by Wilson and Barbas [7], whose only difference from the four

TABLE 1

Span multipliers f_i for $0{\cdot}05 \leqslant \bar{C} \leqslant 2$, $0 \leqslant \bar{D} \leqslant 0{\cdot}1$, and $\theta_T = \pi/2$

No. of spans, N	$i=1$, N	$i=2$, $N-1$	$i=3$, $N-2$	$i=4$, $N-3$	$i=5$, $N-4$
3	0·967	1·065	0·967	–	–
4	0·950	1·050	1·050	0·950	–
5	0·940	1·039	1·041	1·039	0·940
6	0·934	1·032	1·034	1·034	1·032
7	0·929	1·027	1·029	1·029	1·029
8	0·926	1·023	1·026	1·026	1·026
9	0·923	1·020	1·023	1·023	1·023

constraints above was that *bending moments* replaced *deflections* in constraint (4) as the selection criteria for f_i. However, for both straight and curved spans for $N = 3, 4, \ldots, 9$, computations showed that the near-optimal span multipliers for practical cases were always in the range $0{\cdot}85 \leqslant f_i \leqslant 1{\cdot}2$.

Typical numerical results for the span multipliers obeying the four constraints listed above are shown in Table 1. These results, obtained by Threlfall [8] who employed a trial and success procedure to satisfy constraint (4) to within 0·01%, were based on closed form solutions to the static equation counterparts of equations (8) and (9), as presented by Heins [9]. Imposed were the conditions of simply supported extreme ends, zero deflection at all interior supports, and continuity of slope and moment across the interior supports. All of the results in Table 1 are for a curved span with a 90-degree turn, or $\theta_T = \pi/2$. For a fixed N, ranging from 3 to 9, the corresponding row of multipliers stayed the same to within 0·1% when the span parameters $\bar{C}$ and $\bar{D}$ were varied in the practical design ranges $0{\cdot}05 \leqslant \bar{C} \leqslant 2{\cdot}0$ and $0 \leqslant \bar{D} \leqslant 0{\cdot}1$.

5. DYNAMIC RESPONSES

For the dynamic studies, both numerical and experimental, three span configurations were chosen. All three configurations were horizontally curved flat steel plates with a mean radius $R = 2{\cdot}04$ m and cross-section dimensions of $0{\cdot}307 \times 12{\cdot}7$ mm. The first configuration served as the reference span: a single, simply supported curved span with a 30-degree arc, defined by the following parameters

$$N = 1, \qquad \bar{C} = 1{\cdot}6, \qquad \bar{D} = 0, \qquad \bar{T} = 0, \qquad 1/\zeta = 55{\cdot}6, \qquad \theta_T = \pi/6. \quad (17)$$

The second and third configurations were both 3-span units with 90-degree turns: the second with even pier spacing and the third with near-optimal pier spacing, defined by the parameters

$$\begin{gathered} N = 3, \quad \bar{C} = 1{\cdot}6, \quad \bar{D} = 0, \quad \bar{T} = 0, \quad 1/\zeta = 55{\cdot}6, \quad \theta_T = \pi/2; \\ \text{even: } f_1 = f_2 = f_3 = 1, \quad \text{near-optimal: } f_1 = f_3 = 0{\cdot}969, \qquad f_2 = 1{\cdot}063. \end{gathered} \quad (18)$$

The three near-optimal values of f_i in the above equation were measured values (discussed below), and differ only by about 0·2% from the computed values given in the first row of Table 1.

Using the appropriate parameters of equations (17) and (18), the following procedure was used to calculate the peak dynamic responses for the three configurations.;

(1) Compute the time history of the deflection and rotation responses at midspan for the simple curved span, defined by equations (17). Deduce the peak values of each as a function of Ω in the range of zero to one. Use the first six modes and the closed form solutions given in reference [1]. Proceed to the calculations for the two 3-span configurations defined by equations (18).
(2) For the even span case, compute the lowest six frequencies $\bar{p}$ and corresponding mode shapes $\bar{W}_n$ for $n = 1, 2, \ldots, 6$. Use the methods described in the companion paper by Snyder and Wilson [5].
(3) For fixed values of the passage frequency ratio in the range $0{\cdot}1 \leqslant \Omega \leqslant 0{\cdot}8$, compute the corresponding constants defined by equations (11), (12), (13), and (15).
(4) For each Ω, use *Mathematica* with the adaptive Runge–Kutta procedure to solve the differential equations (14) for the time histories of Z_n and Θ_n.
(5) For each Θ, use these solutions to compute the time histories of the dynamic responses $\bar{\eta}$ and $\bar{\beta}$ given by equations (10), located at the midlength of each of the three span segments. Record the co-ordinate pairs $(\Omega, \bar{\eta})$ and $(\Omega, \bar{\beta})$ in which $\bar{\eta}$ and $\bar{\beta}$ are the peak values for a given time history of response. Truncate all sums after mode six.
(6) Repeat the last five steps for the near-optimal case.

Listed in Table 2 are two sets of numerical results: the lowest six normalized free vibration frequencies $\bar{p} = \bar{p}_i$, $i = 1, 2, \ldots, 6$, for each of two 3-span configurations. When the frequencies for like values of i are compared between the two configurations, only small changes in $\bar{p}$ are observed. However, despite these small frequency differences, the differences in the spans' dynamic responses are relatively large, as demonstrated by the following results.

The computed peak midspan deflections $\bar{\eta}$ as a function of Ω are shown in Figures 2(a)–(c) for the even span case, and in Figures 3(a)–(c) for the near-optimal case. Also shown in these figures, for comparison purposes, is the peak dynamic response curve for the simply supported curved reference span whose parameters are defined by equation (17). This reference configuration may be

TABLE 2

First six non-dimensional free vibration frequencies $\bar{p}$ for the two 3-span configuration defined by equation (18)

Pier spacing	$\bar{p}_1$	$\bar{p}_2$	$\bar{p}_3$	$\bar{p}_4$	$\bar{p}_5$	$\bar{p}_6$
Even	0·964	1·251	1·847	3·963	4·525	5·562
Near-optimal	0·956	1·316	1·780	3·891	4·746	5·412

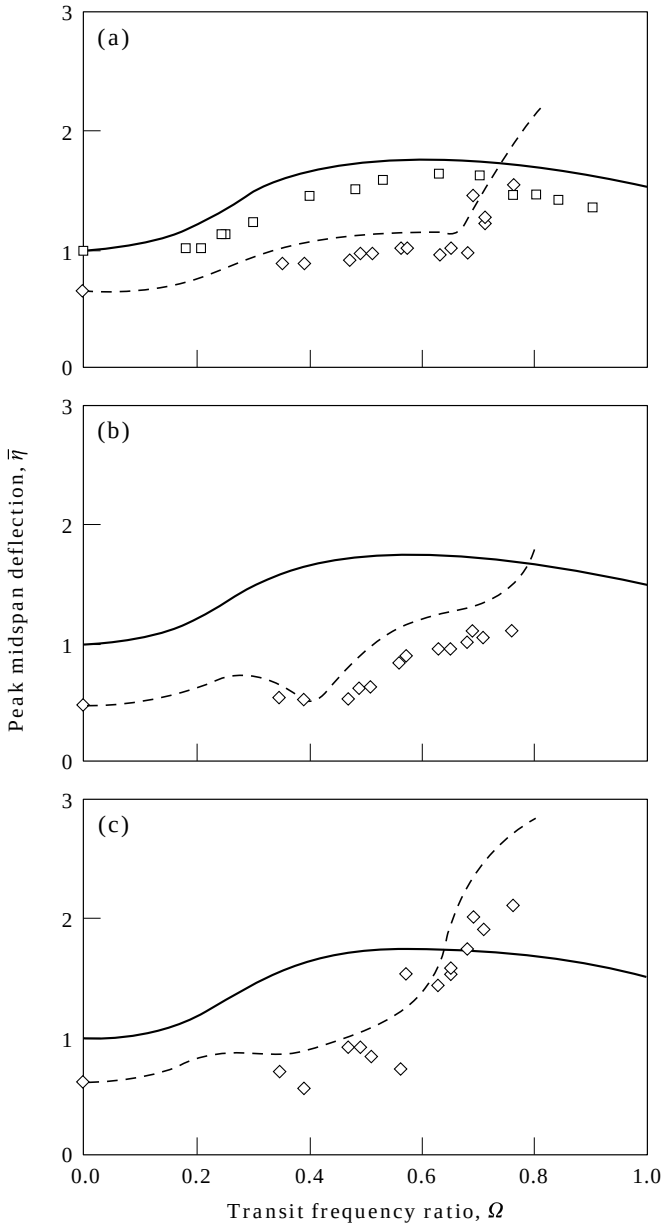

Figure 2. Computed and measured values for the peak dynamic deflection responses for the simple curved reference span defined by equation (17), and for the 3-span configuration with even pier spacings defined by equation (18): (a) entrance span l, (b) middle span 2, and (c) exit span 3. The data are distinguished by: ——, simple curved span (theory); □, simple curved span (experiment); – – –, even pier spacing (theory); ◇ even pier spacing (experiment).

considered as three identical, simple curved spans end-to-end, which altogether form a 90° horizontal curve of the same length as the two types of continuous spans. It is noted that, since the peak midspan static deflection of the simple curved span was calculated to be within 5% of η_s defined by equation (3) for of the straight span counterpart, then $\bar{\eta}$ is not distinguishable from unity on these

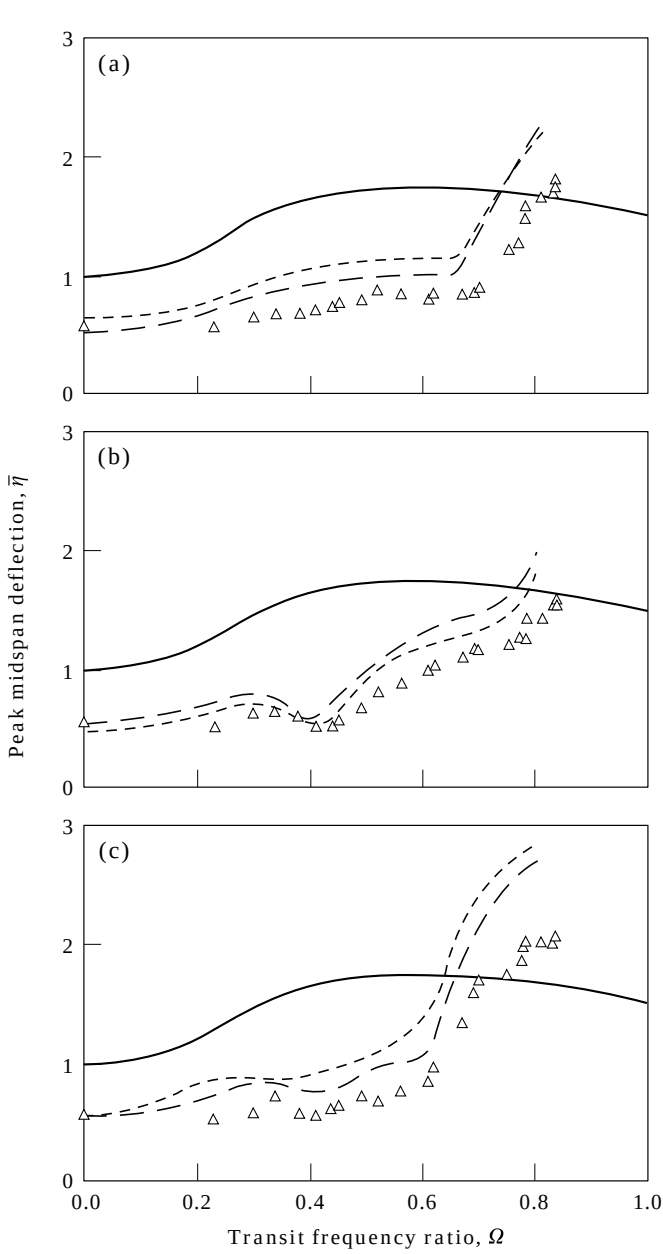

Figure 3. Computed peak dynamic deflection responses for the simple curved reference span, and for the two 3-span configurations: (a) entrance span 1, (b) middle span 2, and (c) exit span 3. The data are distinguished by: ——, simple curved span (theory); – – –, even pier spacing (theory); — — —, near-optimal pier spacing (theory); △, near-optimal pier spacing (experiment).

figures. When all of these data are compared at a fixed Ω, the most important observed results are as follows.

(1) The crossover points at which the peak responses of the continuous spans just reach that of the simple span always occur at $\bar{\eta} \approx 1{\cdot}7$.

(2) Span 3 or the exit span is the critical one for both continuous configurations for two reasons: crossover occurs at the lowest value of $\Omega(=0{\cdot}62$ and $0{\cdot}65)$ for spans 3, compared to Ω $(=0{\cdot}75$ to $0{\cdot}8)$ for spans 1 and 2; and the responses are the highest for spans 3 after crossover, as Ω approaches 0·8.

(3) For $0 \leqslant \Omega \leqslant 0{\cdot}5$, the peak responses of the near-optimal configuration are 45 to 50% less that of the simple span counterpart.

(4) For critical spans 3, and for $0 \leqslant \Omega \leqslant 0{\cdot}8$, the peak responses for the near-optimal configuration are always less than those for the even configuration; see Figure 3(c).

Following the same procedures as in the calculation of $\bar{\eta}$, the companion rotation responses $\bar{\beta}$, of equation (10) were also calculated and then cast in the alternate form

$$\beta/\beta_s = (\bar{\beta}/\beta_s)(\eta_s/R). \tag{19}$$

Here, β_s is the static midspan rotation of the simple curved span defined by equation (17), with a load P applied at midlength. β_s may be calculated for the load at crawl speed or directly from the closed form result; equation (32b) of Tan and Shore [1]. When the results for β/β_s were plotted in the same manner as the responses of Figures 2 and 3, those results were nearly indistinguishable from the results for $\bar{\eta}$ in those figures. Thus, for all practical purposes, β/β_s may replace $\bar{\eta}$ in those figures; and all of the conclusions for span deflection listed above also apply for span rotation.

6. THE EXPERIMENTAL SYSTEM DESIGN

An experimental system was designed and implemented for the purpose of validating the theoretical predictions for curved span responses. A schematic view of a 90-degree continuous span, together with some design details of the point transit load and the span, are shown in Figure 4. The 30-degree simple span, not shown, was also implemented. The experimental curved span system, implemented by Schichtel [10], was a modified version of the experimental straight span system described in detail by Wilson [11]. For the sake of completeness, the span design, the transit load, the propulsion system, and the measuring system are briefly described.

The three span configurations with the characteristics defined by equations (17) and (18), were flat, horizontal steel plates with dimensions such that they behaved as curved beams. That is, the ratio of the spans' width of cross-section (0·127 m) to mean radius R (2·04 m) was 0·0622, well within the limit ratio of 0·2 above which flat plate dynamics become important, according to Wilson and Garg [12]. The span configurations were simply supported at the extreme ends and were held down with hooks at each support, as shown in Figure 4. The spans were prebent so that they were flat and horizontal, or very nearly so, under the added mass of the brass rods hung under the spans. With this added mass, the spans' fundamental frequencies p_1 were measured: 3·65 Hz (22·9 rad/s)

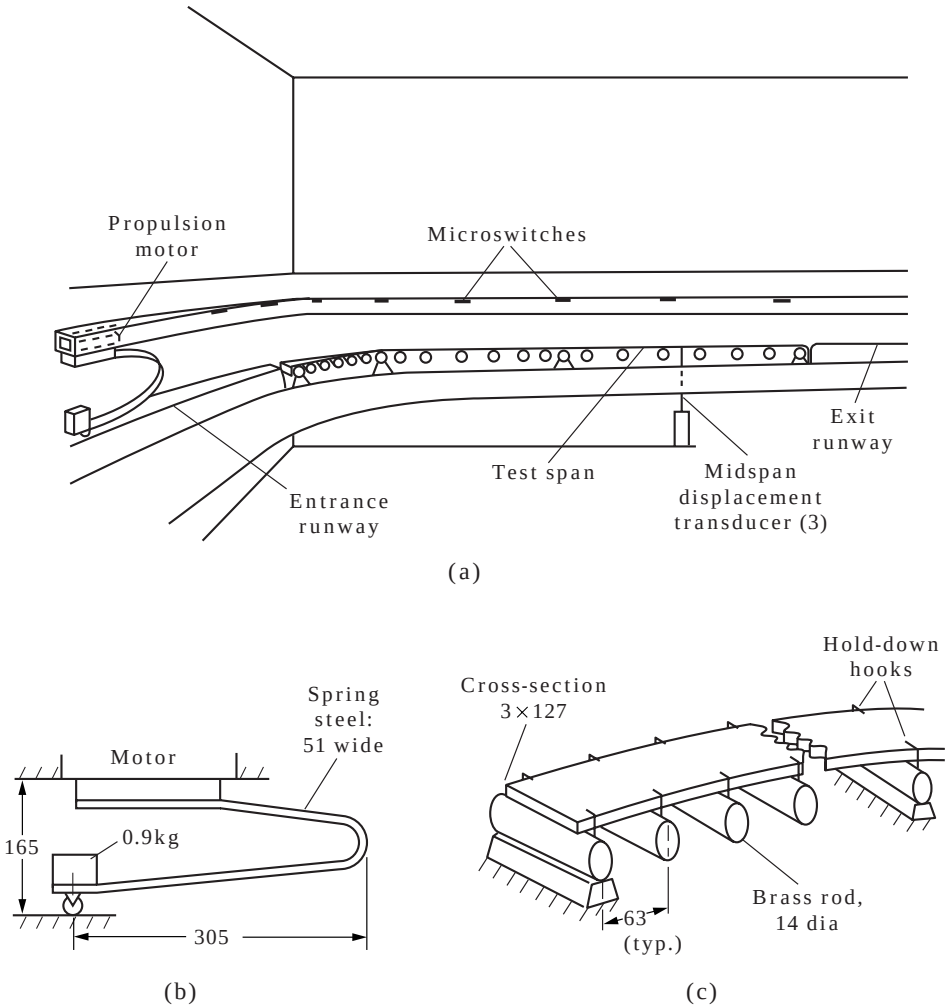

Figure 4 The experimental system showing: (a) overall view of the 90-degree curve; (b) the point load model; and (c) the span detail. Dimensions in mm.

for both the simple span and for the even span configurations; and 3·68 Hz for the near-optimal span.

The transit load was a single-wheeled, 1-kg bogie that maintained good span contact with the help of the prebent steel leaf spring between the bogie and its propulsion motor that gave an added spring load of about 4 N. The propulsion motor was a specially designed linear induction motor that achieved constant speed v on the entrance runway prior to entering the test span. The motor had a 120-Hz voltage supply, and the voltage was preset in the range of 50 to 280 V to achieve the desired constant speed in the range of 1·2 to 7 m/s. This speed was measured for each test run by recording electronically the time of arrival of the motor as it tripped each consecutive microswitch in passing; see Figure 4. The experimental system was designed to achieve a maximum transit frequency ratio of 0·9, which is computed from equation (5) with $p_0 \approx p_1$, or: $\Omega = \pi v/(Lp_0) = \pi(7)/(1{\cdot}07)(22{\cdot}9) \approx 0{\cdot}9$. In reality, values of Ω only up to 0·8 could be

achieved, since higher values caused the bogie to bounce a little on the test spans.

In addition to measuring the speed of the transit load, the time history of each midspan deflection η and of each midspan cross-section rotation β were also recorded. Non-intrusive LVDT's (linear variable differential transformers) were used to measure η; and differential vertical midspan displacements at the inner and outer radius, divided by the cross-section width, were used to measure β. Auxiliary equipment used for these measurements, and also for measurements of the bogie velocity (signals from the tripped microswitches) were signal conditioners and a multiple channel strip chart recorder.

7. DISCUSSION

Consider first the experimental results. For the simple curved span, the peak measured responses are shown as the box points in Figure 2(a), all normalized by the static deflection for the bogie placed at midspan. That same reference deflection was used to normalize the data for the two 3-span configurations. For the simple curved span, the experimental data follow the trend of the predicted results, but are consistently depressed from the predicted results by about 10%. This same trend is also apparent for the continuous spans: data in Figures 2(a)–(c) for the continuous, even spans, and data in Figures 3(a)–(c) for the near-optimal spans. Although system damping may account for a part of the depressed measured responses, (span damping was measured to be about 2% of critical), the main reason that the measured responses are lower than the predicted ones, especially as Ω approaches the 0·8 for the continuous configurations, is the inertia effect of the 1 kg transit mass. Inertia effects are amplified at increasing transit speed. It is recalled that the predictions are all based on a *constant, inertialess, moving force*, a condition that is difficult to achieve experimentally with a moving mass, even though this mass is only about one-seventh the mass of any single span.

Not presented here, for the sake of brevity, are the experimental results for span rotations. Again, and as for the theory, the measured responses for β/β_s were essentially the same as the corresponding measured responses for $\bar{\eta}$ of Figures 2 and 3. Further, in the experimental system, $\beta_s \approx 0{\cdot}02$ rad, which compares favorably with the theoretical value computed from the theory of Tan and Shore [1], equation (32b), provided that the typographical error in their equation (12) is corrected.

Consider the analysis and its application to design. Because the governing equations and the computed peak dynamic responses were cast in terms of non-dimensional system parameters, the results of this analysis may be especially useful in the efficient design of curved, elevated guideway structures for future rapid transit systems. For instance, consider this example. The preliminary design of a closed box guideway similar to that of Figure 1 is based on a simple straight span, 30 m in length, which accommodates the static loading of a vehicle that is much shorter than 30 m and has a mass much less than that of the span. The fundamental frequency of this simple span, computed from equation

(3), is $p_0 = 18{\cdot}85$ rad/s or 3 Hz. It is proposed to use this preliminary design as a basis for the following curved span that has nearly the same system parameters as those of equation (18): a uniform, 3-span guideway with a 90-degree turn; a near-optimal pier spacing; and a mean arc length between piers of $L = 30$ m ($R = 57{\cdot}3$ m). One key question concerning the dynamic design of the curved span counterpart is: what would be the maximum allowable speed of the vehicle, assuming sufficient side restraints while traversing the curve?

To answer this, refer to the peak response curves for the near-optimal spans shown in Figures 3. Choose $\bar{\eta}$ as unity and read the corresponding highest value of the transit frequency ratio on these three curves, or $\Omega \approx 0{\cdot}5$ from Figures 3(b) and (d). From the definition of Ω, equation (5), the critical or maximum vehicle speed for the curved span is $v = 0{\cdot}5Lp_0/\pi = 90$ m/s.

8. CONCLUSIONS

Three main conclusions of this study are: (1) for the illustrations of 3-span continuous configurations with 90-degree curves and zero warping (closed cross-sections), the critical (or exit span) dynamic responses for near-optimal pier spacings are less than those for even pier spacings, results that are analogous to the cases of straight continuous spans reported by Wilson and Barbas [7]; (2) although the effects of transit torque $\bar{T}$ on continuous spans are not illustrated herein, and this may bear future investigation, it is expected that $\bar{T}$ will affect the critical responses only as Ω approaches unity, as was the case reported by Wilson *et al.* [13] for simple spans with parameters close to those of equations (17); and (3) the experimental results do complement the predicted responses and give credibility to Vlasov's mathematical model for curved spans in which a constant moving force (no inertial effects of the transit load) gives a high estimate of the critical dynamic responses.

ACKNOWLEDGMENTS

This research was sponsored in part by the U.S. Department of Transportation, contract No. DOT-OS-60130. The authors thank Adam J. Schichtel for his assistance with the experiments.

REFERENCES

1. C. P. TAN and S. SHORE 1968 *Journal of the Structural Division, ASCE* **94**, 761–781. Dynamic response of a horizontally curved bridge.
2. V. Z. VLASOV 1961 *National Science Foundation Technical Report*. Thin-walled beam theory.
3. D. Z. HUANG, T. L. WANG and M. SHAHAWAY 1998 *Computers and Structures* **68** 513–528. Vibrations of horizontally curved box girder due to vehicles.
4. D. Z. HUANG, T. L. WANG and M. SHAHAWAY 1992 *Computers and Structures* **57** 703–714. Dynamic behavior of horizontally curved I-girder bridges.
5. J. M. SNYDER and J. F. WILSON 1992 *Journal of Sound and Vibrations* **157**, 345–355. Free vibrations of continuous horizontally curved beams.

6. D. A. NETHERCROFT, P. R. SLATER and A. S. MALIK 1989 *Steel Construction Institute Publication 057*, 1–121. Design of members subject to combined bending and torsion.
7. J. F. WILSON and S. T. BARBAS 1982 *Journal of Advanced Transportation* **16**, 253–283. Dynamics of near-optimal spans with moving loads.
8. I. THRELFALL 1996 *Master's Project, Department of Civil and Environmental Engineering, Duke University*, 1–68. Continuous horizontally curved spans: optimal pier spacings.
9. C. P. HEINS 1975 *Bending and Torsional Design of Structural Members*. Lexington, MA: Lexington Books.
10. A. J. SCHICHTEL 1984 *Master's Project; Department of Civil and Environmental Engineering, Duke University*, 1–27. Experiments on curved span dynamics.
11. J. F. WILSON 1977 *Journal of the Engineering Mechanics Division, ASCE* **103**, 701–715. Model experiments for span-vehicle dynamics.
12. J. F. WILSON and D. P. GARG 1978 *AIAA Journal* **16**, 270–272. Frequencies of annular plate and curved beam elements.
13. J. F. WILSON, C. BIRNSTIAL, C. W. DOLAN, P. E. POTTER and P. R. SPENCER 1985 *Journal of Structural Engineering* **111**, 1873–1898. Dynamics of steel elevated guideways.